Catalysis Today xxx (xxxx) xxx

Contents lists available at ScienceDirect

Catalysis Today

journal homepage: www.elsevier.com/locate/cattod

Molybdenum oxide as an efficient promoter to enhance the NH_3-SCR performance of CeO_2-SiO_2 catalyst for NO_x removal

Wei Tan [a,b], Jin Wang [c], Yandi Cai [a], Lulu Li [a,d], Shaohua Xie [b], Fei Gao [a,*], Fudong Liu [b,*], Lin Dong [a]

[a] Key Laboratory of Mesoscopic Chemistry of MOE, School of Chemistry and Chemical Engineering, Jiangsu Key Laboratory of Vehicle Emissions Control, School of Environment, Center of Modern Analysis, Nanjing University, Nanjing 210093, PR China
[b] Department of Civil, Environmental, and Construction Engineering, Catalysis Cluster for Renewable Energy and Chemical Transformations (REACT), NanoScience Technology Center (NSTC), University of Central Florida, Orlando, FL 32816, United States
[c] State Key Laboratory of Analytical Chemistry for Life Sciences, School of Chemistry and Chemical Engineering, Nanjing University, Nanjing 210023, PR China
[d] School of Environmental and Chemical Engineering, Jiangsu University of Science and Technology, Zhenjiang 212003, PR China

ARTICLE INFO

Keywords:
Low-temperature NH_3-SCR activity
SO_2 resistance
Mo doping
Ce-Si mixed oxide
Improved redox properties and surface acidity

ABSTRACT

Selective catalytic reduction (SCR) of NO_x with NH_3 has been widely used for the removal of NO_x. Because of the inevitable disadvantages of conventional V_2O_5-$WO_3(MoO_3)/TiO_2$ catalysts such as poor low-temperature SCR activity and toxicity of vanadium, as well as the high-cost and over-strong NH_3 adsorption of zeolite catalysts, the development of efficient and non-toxic metal oxide SCR catalysts is highly demanded. Previously, we have developed an environmentally-benign CeO_2-SiO_2 mixed-oxide SCR catalyst ($CeSi_2$), which exhibited superior SO_2 resistance ability. However, the low-temperature SCR activity on $CeSi_2$ was not that satisfactory. In this work, we proposed a new strategy of Mo doping to improve the low-temperature SCR activity on $CeSi_2$, which was very crucial for its practical application. By a simple co-precipitation method, a homogenous Mo-Ce-Si mixed-oxide catalyst was prepared. The Mo doping could significantly enhance the NH_3-SCR activity on $CeSi_2$ below 250 °C, and the optimal catalyst was $Mo_{0.1}CeSi_2$, which could achieve 80% NO_x conversion at 200 °C. $Mo_{0.1}CeSi_2$ also exhibited superior N_2 selectivity and resistance to SO_2/H_2O poisoning. Via a series of characterizations, it was found that the redox properties and surface acidity on $CeSi_2$ by Mo doping, which accounted for the enhanced low-temperature NH_3-SCR activity on $Mo_{0.1}CeSi_2$. The reaction mechanism on $Mo_{0.1}CeSi_2$ was also fully revealed by *in situ* DRIFTS experiments. This work provided a new insight for the development of efficient low-temperature SCR catalysts with superior SO_2 resistance ability.

1. Introduction

With the increasing demand for fossil fuels in human society, the harmful gas emission from various plants and engines has resulted in serious air pollution [1]. Among these air pollutants, nitrogen oxides (NO_x) have drawn great attention because they may induce major air pollution problems (photochemical smog, haze and acid rain, *etc.*) [2]. Selective catalytic reduction (SCR) by injected reductants is considered as one of the most efficient techniques for NO_x removal [3,4]. Among them, SCR of NO_x with NH_3 (NH_3-SCR of NO_x) has been recognized as a low-cost but efficient technology for the removal of NO_x [5,6]. As is well known, one of the research cores in the energy and environmental catalysis field is the catalyst. Improving the existing catalysts or develop novel catalysis materials are common strategies [7–11]. To meet the tightened emission control standard, many efforts have been devoted to developing novel NH_3-SCR catalysts with improved activity and better resistance to poisoning [4,12,13].

Due to the biological toxicity and relatively poor low-temperature activity of the state-of-art vanadium-based NH_3-SCR catalyst, designing an efficient vanadium-free catalyst is highly demanded [14]. Among all the candidates, CeO_2 has attracted much interest for its superior redox property and environmentally friendly features [15–20]. Recently, we reported a novel Ce-Si mixed-oxide catalyst with enhanced NH_3-SCR activity and superior resistance to SO_2/H_2O poisoning, while the low-temperature NH_3-SCR activity on this Ce-Si mixed-oxide catalyst still needs to be further promoted [21]. Typically, improving the

* Corresponding authors.
E-mail addresses: gaofei@nju.edu.cn (F. Gao), fudong.liu@ucf.edu (F. Liu).

https://doi.org/10.1016/j.cattod.2021.07.007
Received 31 March 2021; Received in revised form 12 June 2021; Accepted 3 July 2021
Available online 10 July 2021

surface acidity was one of the most common but effective strategies to boost the NH_3-SCR activity on CeO_2-based materials [22–26]. For example, WO_3 modification has been proved to be an effective method to promote the deNO_x efficiency of CeO_2/TiO_2 catalysts [27,28]. Zhao et al. proposed a Zr doping strategy to improve the surface acidity of $CeVO_4$ catalyst, by which the NH_3-SCR activity and N_2 selectivity were significantly promoted [29]. It was also found that sulfation treatment on CeO_2 could dramatically enhance its surface acidity, then contribute to the enhancement of NH_3-SCR activity [20,26,30–32]. For Ce-Si mixed-oxide catalyst, abundant surface hydroxyl groups could serve as the Brønsted acid sites. However, the acid strength of the Brønsted acid sites on the Ce-Si mixed-oxide catalyst was still relatively weak [21], which restricted the further improvement of catalytic activity. As has been widely reported, to further tune the acidity of a catalyst, modifying it with some other transition metal oxides (WO_3, Nb_2O_5 and MoO_3, *etc*.) could be effective [22,24,33–41]. Previously, it was found that the well-dispersed Mo species in CeO_2-based catalysts could act as efficient acid sites for NH_3 adsorption and activation [42,43]. Moreover, Mo could facilitate the redox properties and the SO_2/H_2O/arsenic-resistance of CeO_2 based materials [44–46]. Therefore, MoO_3 doped Ce-Si mixed oxides could be a promising catalyst with enhanced low-temperature activity and superior resistance to SO_2/H_2O poisoning.

Herein, aimed at broadening the operating temperature window of Ce-Si mixed-oxide catalyst to lower temperatures and maintaining the superior resistance to SO_2 poisoning at the same time, a Mo-doping strategy was adopted. The Ce-Si mixed oxide doped with optimal doping amount of Mo presented satisfactory low-temperature (~200 °C) activity together with almost 100% N_2 selectivity in the operating temperature window (200–400 °C). It also performed excellent NO conversions (>85%) even after being exposed to 500 ppm SO_2 at 225 °C. Via a series of characterizations, it was found that the Mo doping could greatly promote the redox properties and surface acidity of Ce-Si mixed oxides, which accounted for the higher low-temperature NH_3-SCR activity on Mo doped Ce-Si mixed oxides catalysts.

2. Material and methods

2.1. Catalyst preparation

The CeO_2-SiO_2 mixed oxide was prepared by a coprecipitation method reported elsewhere [21]. In details, 0.05 mol $(NH_4)_2Ce(NO_3)_6.6H_2O$ was dissolved in 200 mL ethanol to obtain a homogenous solution. After that, 0.1 mol tetraethyl orthosilicate (TEOS) was added dropwise into the ethanol solution of $(NH_4)_2Ce(NO_3)_6$ under vigorous magnetic stirring. Keep stirring for 30 min and then aqueous ammonia ($NH_3{\cdot}H_2O$, 25%) was added dropwise into the mixture until the pH reached 10. The resulting precipitations were aged overnight, filtered, and washed with distilled water. The obtained gel was desiccated at 100 °C for 12 h and finally calcined at 550 °C for 4 h in air, with a ramping rate of 5 °C/min. The prepared sample was denoted as $CeSi_2$. For the preparation of Mo doped CeO_2-SiO_2 catalysts, a certain amount of ammonium molybdate ($(NH_4)_6Mo_7O_{24}.4H_2O$) and 0.05 mol $(NH_4)_2Ce(NO_3)_6.6H_2O$ were co-dissolved in 200 mL ethanol to obtain a homogenous solution with Mo-Ce molar ratio of a:1 (a = 0.01, 0.05, 0.1, 0.25 and 0.5). The following procedures were just the same as the preparation of $CeSi_2$. The obtained samples were denoted as Mo_aCeSi_2. CeO_2 prepared by a precipitation method was also used as a reference. For further characterizations, all samples were grounded into fine powder for use.

2.2. Characterizations

The specific surface areas of the prepared catalysts were calculated from N_2 adsorption-desorption isotherms at −196 °C by the Brunauer-Emmett-Teller (BET) method on a Micromeritics ASAP-2020 analyzer. Before the test, the catalysts were degassed at 300 °C for 4 h.

Powder X-ray diffraction (XRD) patterns of the catalysts were collected on a Philips X′pert Pro diffractometer equipped with a Ni-filtered Cu Kα radiation (0.15408 nm). The range of 2θ was 10° - 80° with a scanning speed of 10°/min. The step size was set at 0.02°.

Raman spectra of the catalysts were collected on LabRAM Aramis (Japan Horiba) Laser Raman spectrometer with an Ar^+ laser beam with an emission line at 532 nm. The power output was set at 10 mW.

The transmission electron microscopy (TEM) and the energy dispersive spectroscopy (EDS) elemental mapping images were obtained from a JEOL 2800 instrument equipped with a dual-type EDS detector.

X-ray Photoelectron Spectroscopy (XPS) experiments were performed on a PHI 5000 Versa Probe system equipped with a monochromatic Al X-ray radiation source (1486.6 eV) with an accelerating power of 15 kW. Binding energies (BE) of all the elements were calibrated with C 1s line at 284.6 eV.

H_2-temperature-programmed reduction (H_2-TPR) experiments were performed on a quartz U-tube reactor connected to a thermal conductivity detector (TCD). In each measurement, *ca.* 10 mg of the catalyst was first pretreated in flowing N_2 (30 mL/min) at 200 °C for 1 h and then cooled down to room temperature. Then the temperature was raised from 100 °C to 900 °C linearly with a ramping rate of 10 °C/min in a flow of 7 vol% H_2/Ar (30 mL/min).

NH_3-temperature-programmed desorption (NH_3-TPD) was carried out in a fixed-bed quartz tube reactor connected to an online Thermo Nicolet iS10 FTIR spectrometer equipped with a 2 m path-length gas cell (250 mL volume). Before the test, *ca.* 100 mg samples were pretreated in a flow of Ar (100 mL/min) at 300 °C for 30 min. Then the samples were cooled to room temperature and exposed to a flow of 1000 ppm NH_3/Ar (100 mL/min) to saturation, followed by Ar purge for 30 min. After that, the samples were heated linearly to 600 °C with a ramping rate of 5 °C/min.

In situ diffuse reflectance infrared Fourier transform spectroscopy (*in situ* DRIFTS) experiments were performed on an FTIR spectrometer (Nicolet Nexus 5700) equipped with an MCT detector cooled by liquid N_2. Before the test, samples were pretreated in flowing air at 450 °C for 1 h. Background spectra were then collected in a flowing high-purity N_2 stream as the powder samples cooled to the target temperature, and the backgrounds of samples would be subtracted from the sample spectrum automatically. The feeding gas (50 mL/min) contained 3000 ppm NH_3 (when used), 3000 ppm NO (when used), 5 vol% O_2 (when used) and N_2 balance. All spectra were collected from 400 to 4000 cm^{-1} recorded by accumulating 32 scans, with a resolution of 4 cm^{-1}.

2.3. Catalytic performance measurements

NH_3-SCR and NO/NH_3 oxidation activity on the prepared samples were tested on a fixed-bed quartz tube reactor. Before the test, catalysts were pressed into tablets and sieved to 40–60 mesh. The feed gas was composed of 500 ppm NO (when used), 500 ppm NH_3 (when used), 5 vol % O_2, 200/500 ppm SO_2 (when used), 5% H_2O and N_2 balanced. The total flow rate was 200 mL/min, giving a weight hourly space velocity (WHSV) of 48,000 $mL{\cdot}g^{-1}{\cdot}h^{-1}$ (Gaseous hourly space velocity (GHSV) was approximately 90,000 h^{-1}). The concentration of NO, NO_2, N_2O and NH_3 in the effluent gas was analyzed by an FTIR spectrometer (Thermo Nicolet iS10) equipped with a 2 m path-length gas cell (200 mL volume). The NO_x conversion and N_2 selectivity were calculated according to the following formulas:

$$NO\quad conversion\quad =\quad \frac{[NO]_{in}-[NO]_{out}}{[NO]_{in}}\times 100\%$$

$$N_2\quad selectivity = \frac{[NO]_{in}+[NH_3]_{in}-[NO]_{out}-[NH_3]_{out}-[NO_2]_{out}-2[N_2O]_{out}}{[NO]_{in}+[NH_3]_{in}-[NO]_{out}-[NH_3]_{out}}\times 100\%$$

The NH_3 conversion in NH_3 oxidation reaction and NO conversion in NO oxidation reaction were determined by the following equations:

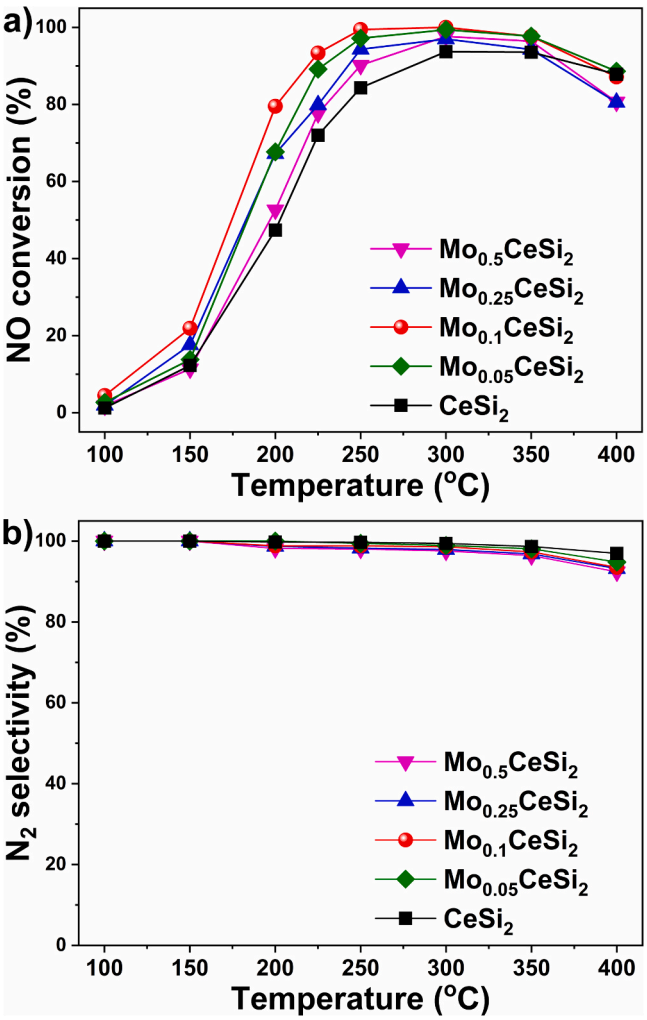

Fig. 1. a) NO conversions and b) N_2 selectivity in NH_3-SCR reaction on $CeSi_2$ and Mo_aCeSi_2 catalysts ($a = 0.01$, 0.05, 0.1, 0.25 and 0.5).

$$NH_3 \quad conversion \quad = \quad \frac{[NH_3]_{in} - [NH_3]_{out}}{[NH_3]_{in}} \times 100\%$$

$$NO \quad conversion \quad = \quad \frac{[NO]_{in} - [NO]_{out}}{[NO]_{in}} \times 100\%$$

3. Results and discussion

3.1. NH_3-SCR catalytic performance

The NH_3-SCR activity and N_2 selectivity on Mo_aCeSi_2 were tested to investigate the influence of Mo doping on the NH_3-SCR performance of $CeSi_2$. As illustrated in Fig. 1a, with the increase of the Mo doping, the NH_3-SCR activity was promoted and reached the best low-temperature activity on $Mo_{0.1}CeSi_2$, with a NO conversion of 80% at 200 °C under the WHSV of 48,000 $mL \cdot g^{-1} \cdot h^{-1}$, much higher than that of $CeSi_2$ (47%). A broader operating temperature window (200–400 °C) was also achieved on $Mo_{0.1}CeSi_2$. Moreover, as reported previously, $CeSi_2$ exhibited a satisfactory N_2 selectivity [21]. As shown in Fig. 1b and Table S1, on the Mo doped $CeSi_2$ catalyst, the high-level N_2 selectivity (>90%) was well maintained. The superior low-temperature activity and N_2 selectivity made $Mo_{0.1}CeSi_2$ a promising catalyst for the application in industrial flue gas $DeNO_x$ at a low-temperature range. A reference catalyst of Mo supported on $CeSi_2$ ($Mo_{0.1}/CeSi_2$, with a molar ratio of Mo: Ce = 0.1) was also tested in its NH_3-SCR activity. As shown in Fig. S1,

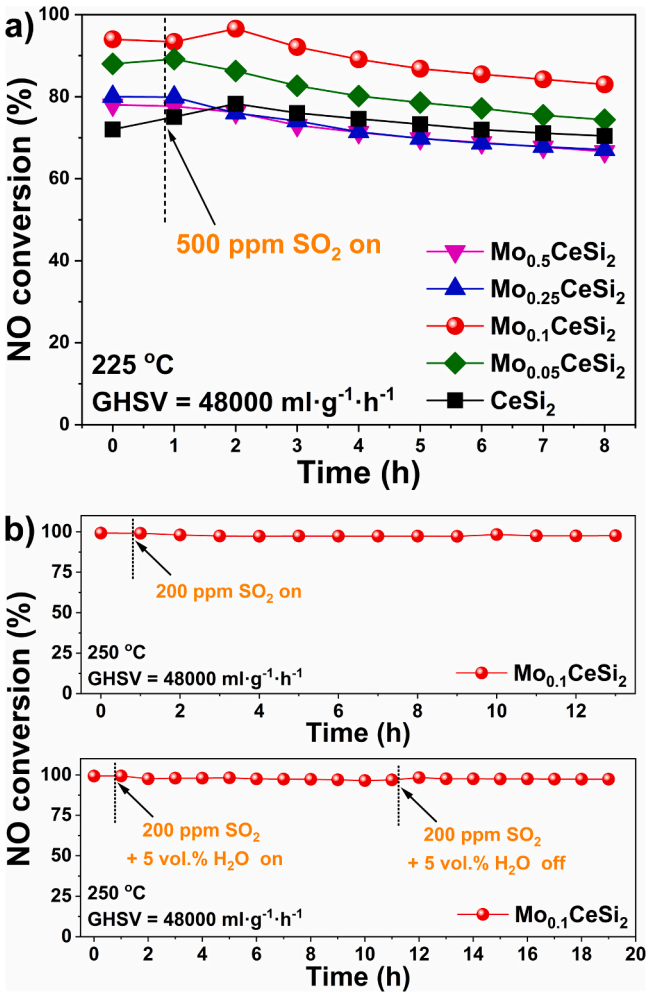

Fig. 2. a) NO conversions on $CeSi_2$ and Mo_aCeSi_2 catalyst in the presence of 500 ppm SO_2 at 225 °C; b) NO conversions on $Mo_{0.1}CeSi_2$ catalyst in the presence of 200 ppm SO_2 + 5 vol% H_2O at 250 °C.

the operating temperature window of $Mo_{0.1}CeSi_2$ was much broader than that of $Mo_{0.1}/CeSi_2$. In the following sections, we would try to reveal the promoting effect of Mo doping on the NH_3-SCR catalytic performance of $CeSi_2$.

3.2. Influence of H_2O and SO_2

The resistance to SO_2 and H_2O was an important performance indicator of NH_3-SCR catalysts aimed at industrial applications. The SO_2/H_2O resistance ability of Mo_aCeSi_2 was evaluated through a long-time test in the presence of SO_2 and H_2O. As shown in Fig. 2a, $CeSi_2$ and $Mo_{0.1}CeSi_2$ exhibited excellent resistance to SO_2 (500 ppm) even at 225 °C. Only a slight decline in their NO conversions was observed in 8 h. Although $CeSi_2$ showed great resistance to SO_2-poisoning, the NO conversion of it was relatively lower at low-temperature range (≤70% at 225 °C). Via Mo doping, the low-temperature activity on $CeSi_2$ was improved, the excellent SO_2 resistance of the $CeSi_2$ catalyst was fully maintained. To further estimate the SO_2/H_2O resistance ability of $Mo_{0.1}CeSi_2$, the NH_3-SCR activity on $Mo_{0.1}CeSi_2$ was tested in the presence of 200 ppm SO_2 + 5 vol% H_2O at 250 °C (Fig. 2b). Almost no inhibition effect was observed on $Mo_{0.1}CeSi_2$, which exhibited a high NO conversion (≥90%) throughout the entire test. As shown in Table S2, when compared with the recently reported novel NH_3-SCR catalyst, $Mo_{0.1}CeSi_2$ still performed as one of the best SO_2/H_2O resistance.

Table 1
Data summary on BET surface area, parameters of Raman spectra and surface elemental compositions.

Samples	Specific surface area (m^2/g)	I_D/IF_{2g} [a]	Atomic concentration (%)			
			Ce	Si	O	Mo
CeO_2	55	0.09	21.1	/	78.9	/
$CeSi_2$	163	0.22	12.4	7.6	79.9	/
$Mo_{0.05}CeSi_2$	223	/	9.0	14.6	75.9	0.50
$Mo_{0.1}CeSi_2$	269	0.33	10.3	11.0	77.8	0.84
$Mo_{0.25}CeSi_2$	220	/	11.5	7.6	80.1	0.74
$Mo_{0.5}CeSi_2$	179	/	10.9	8.5	80.0	0.61

[a] Calculated by the ratio of the peak area of D-bands and F_{2g} bands of CeO_2.

3.3. Structural characteristics

As listed in Table 1, after Mo doping, a higher specific surface area was achieved on $Mo_{0.1}CeSi_2$ (269 m^2/g) when compared with $CeSi_2$ (163 m^2/g). The higher specific surface area was always related to more exposed active sites, which might contribute to the enhanced NH_3-SCR activity on $Mo_{0.1}CeSi_2$. The XRD patterns for Mo_aCeSi_2 were also collected (Figs. 3a and S2). Similar to $CeSi_2$, no diffraction peak assigned to crystalline CeO_2 was detected on $Mo_{0.1}CeSi_2$, and no bulk MoO_3 was found, indicating the formation of an amorphous Mo-Ce-Si mixed oxide with highly dispersed CeO_2 and MoO_3 species. The low crystallinity of Mo_aCeSi_2 might contribute to their high specific surface area (>200 m^2/g).

To further investigate the structure of $Mo_{0.1}CeSi_2$, Raman spectra were also collected (Figs. 3b and S3). The band at *ca.* 460 cm^{-1} could be

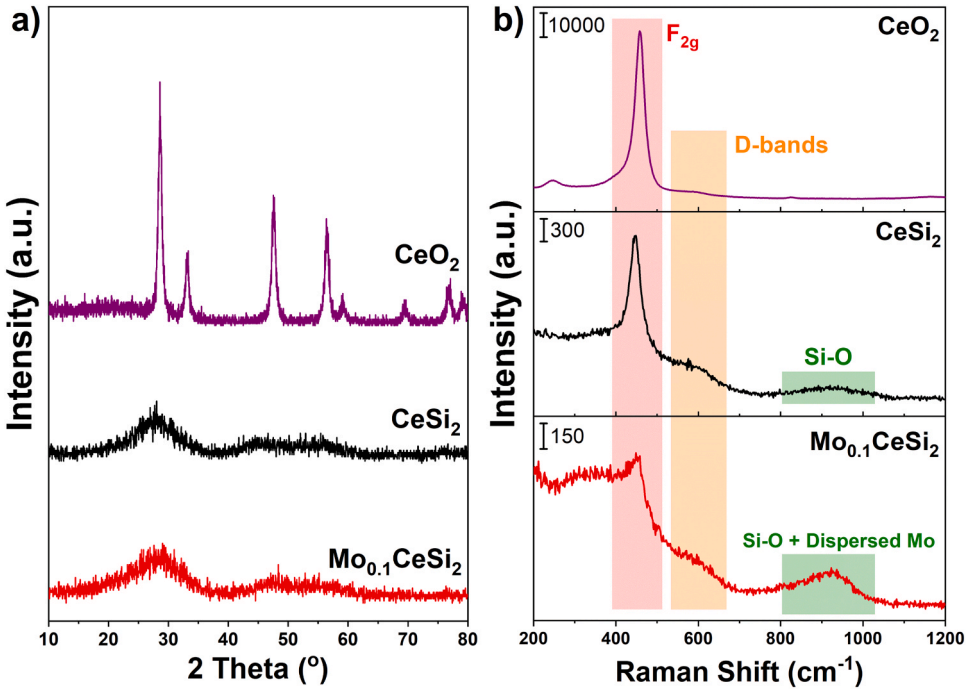

Fig. 3. a) XRD patterns and b) Raman spectra for CeO_2, $CeSi_2$ and $Mo_{0.1}CeSi_2$.

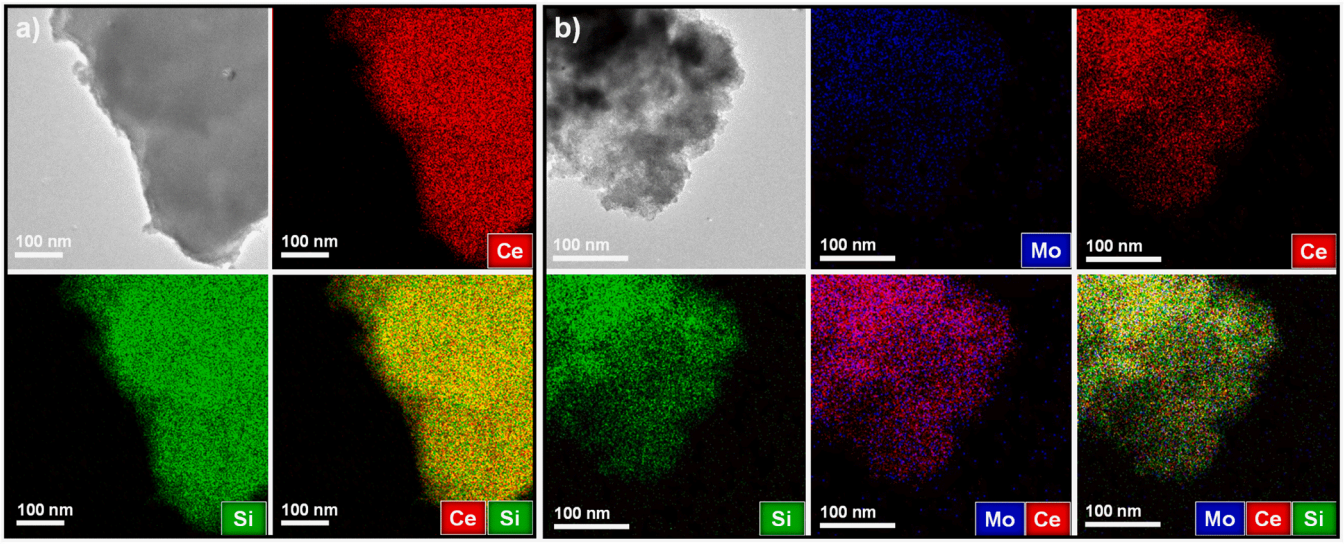

Fig. 4. TEM and EDS-mapping images of a) $CeSi_2$ and b) $Mo_{0.1}CeSi_2$.

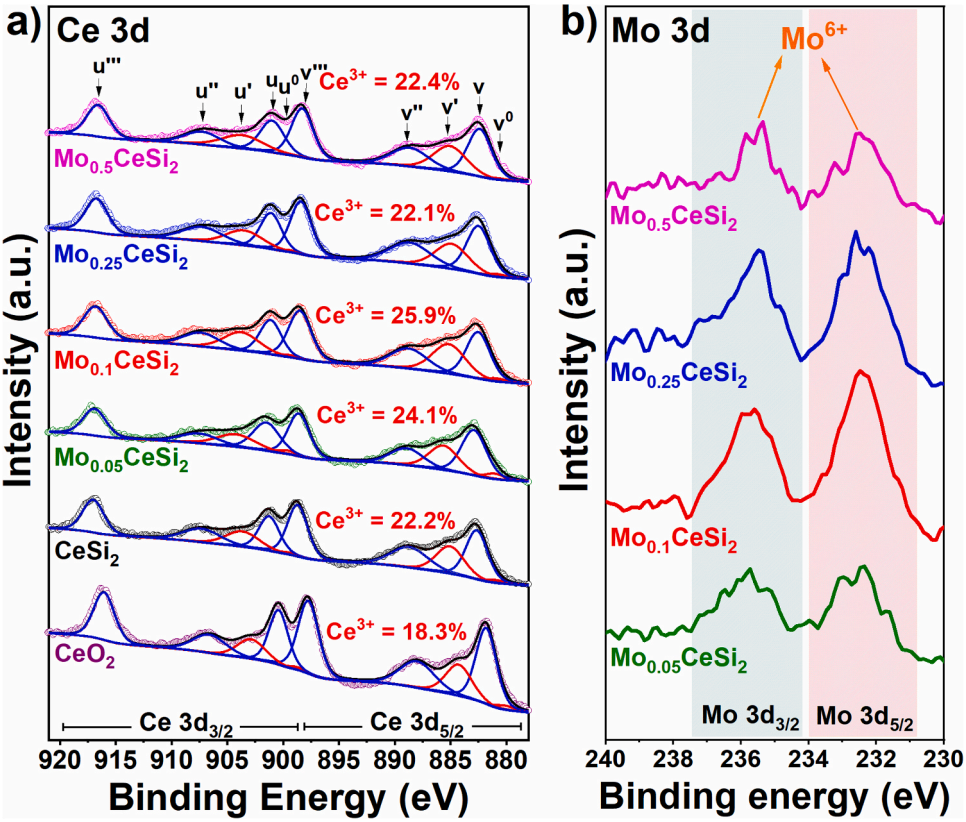

Fig. 5. a) Ce 3d and b) Mo 3d XPS spectra for Mo_aCeSi_2, with CeO_2 and $CeSi_2$ as references.

assigned to the F_{2g} vibration mode of CeO_2 cubic fluorite structure [47, 48]. For $CeSi_2$, the intensity of F_{2g} band on $CeSi_2$ was much lower than that on CeO_2, indicating the lower crystallinity of $CeSi_2$. After being doped with Mo, the intensity of F_{2g} band further decreased. The lowest intensity of F_{2g} bands on $Mo_{0.1}CeSi_2$ suggested its lowest crystallinity (Fig. S3), well explaining the highest specific surface area of $Mo_{0.1}CeSi_2$. The band at *ca.* 590 cm^{-1} was related to the oxygen defects (D-bands),

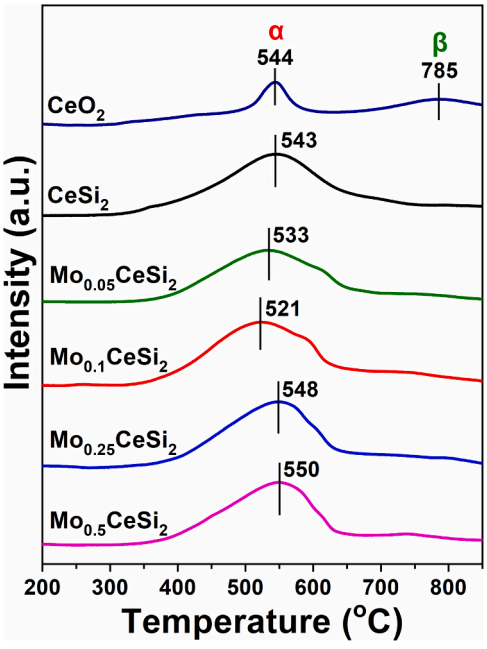

Fig. 6. H_2-TPR profiles of CeO_2, $CeSi_2$ and Mo_aCeSi_2.

and the peak area ratio of D-bands to F_{2g} band (I_D/IF_{2g}) could be used to indicate the relative concentration of oxygen defects on CeO_2 [47,49]. As listed in Table 1, the I_D/IF_{2g} value of $Mo_{0.1}CeSi_2$ was higher than that of $CeSi_2$ and CeO_2, which meant that more oxygen defects formed on $Mo_{0.1}CeSi_2$. Interestingly, a broad band at 800–1000 cm^{-1} was observed on $CeSi_2$, which could be attributed to the symmetric Si-O stretching vibrations. For $Mo_{0.1}CeSi_2$, the relatively more intense bands at 800–1000 cm^{-1} could be attributed to the mixed signals of Si-O species and highly dispersed molybdate species [50–52]. More oxygen defects could significantly promote the redox performance of $Mo_{0.1}CeSi_2$, then facilitate the activation of reactants [49].

TEM and EDS-mapping images of $CeSi_2$ and $Mo_{0.1}CeSi_2$ were also collected. $CeSi_2$ and $Mo_{0.1}CeSi_2$ showed no specific morphology (Fig. S4). As shown in Fig. 4, similar to $CeSi_2$ that Ce and Si were well mixed, the distribution of Mo, Ce and Si in $Mo_{0.1}CeSi_2$ matched well with each other, suggesting the formation of a homogeneous Mo-Ce-Si mixed oxide, and Mo was in a highly dispersed state. It has been reported that highly dispersed MoO_3 species could dramatically promote the NH_3-SCR activity on CeO_2-based materials [53]. The abundant Mo sites on $Mo_{0.1}CeSi_2$ could be one of the main reasons for the enhanced low-temperature NH_3-SCR activity.

The surface chemical states on $Mo_{0.1}CeSi_2$ was investigated by XPS spectra. The surface elemental composition was listed in Table 1. As shown in Fig. 5a, the Ce 3d XPS spectra were resolved into 10 peaks by Gaussian-Lorentz fitting. The peaks marked with u^0, u′, v^0 and v′ were attributed to $3d^{10}4f^1$ state of Ce^{3+} species, while the other peaks were ascribed to $3d^{10}4f^0$ state of Ce^{4+} species [54]. The surface concentration of Ce^{3+} was calculated by the following formula:

$$Ce^{3+}(\%) = \frac{S_u^0 + S_v^0 + S_u' + S_v'}{\sum (S_u + S_v)} \times 100\%$$

Su and Sv were the areas of peaks marked with u and v.

The concentration of surface Ce^{3+} species on $Mo_{0.1}CeSi_2$ (25.9%)

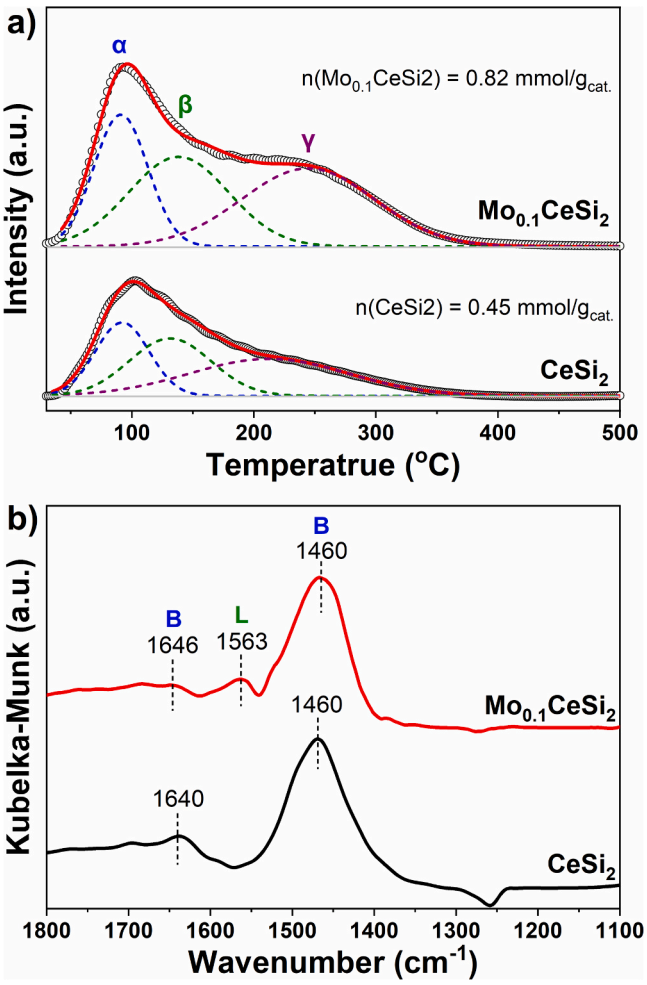

Fig. 7. a) NH_3-TPD profiles for $CeSi_2$ and $Mo_{0.1}CeSi_2$; b) *In situ* DRIFTS of NH_3 adsorption on $CeSi_2$ and $Mo_{0.1}CeSi_2$ (50 °C).

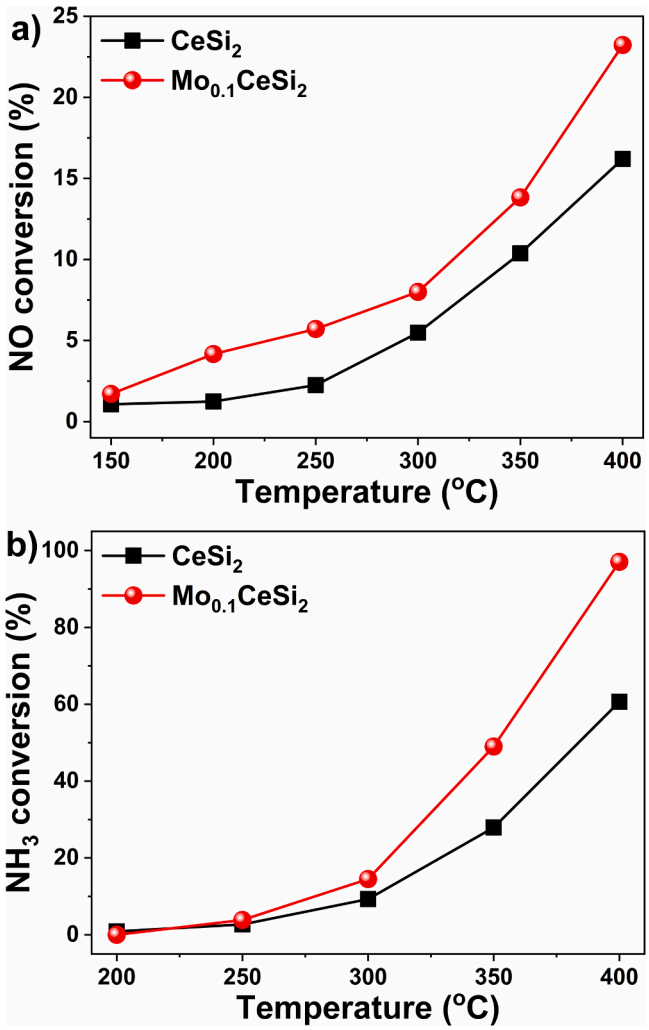

Fig. 8. a) NO conversions in NO oxidation reaction and b) NH_3 conversions in NH_3 oxidation reaction on $CeSi_2$ and $Mo_{0.1}CeSi_2$ catalysts.

was higher than that on $CeSi_2$ (22.2%) and CeO_2 (18.3%), indicating that appropriate Mo doping could facilitate the formation of Ce^{3+} on $CeSi_2$. The higher concentration of surface Ce^{3+} on $Mo_{0.1}CeSi_2$ was beneficial for the activation of reactants, thereby promoting its NH_3-SCR activity. The Mo 3d XPS spectra on $Mo_\alpha CeSi_2$ were also collected (Fig. 5b). Mo species on $Mo_\alpha CeSi_2$ are mainly in Mo^{6+} state [55]. Interestingly, as listed in Table 1, it was found that a higher surface concentration of Mo was observed on $Mo_{0.1}CeSi_2$ despite of its lower Mo doping amount than that on $Mo_{0.25}CeSi_2$ and $Mo_{0.5}CeSi_2$, indicating the best dispersion of Mo species on $Mo_{0.1}CeSi_2$. As shown in Fig. S5a, the peak at *ca.* 102.5 eV could be assigned to Si^{4+} species [56]. The shift of the Si 2p to lower binding energy as well as the shift of the O 1s XPS peak of lattice oxygen species to higher binding energy on $Mo_\alpha CeSi_2$ further supported the argument that a strong interaction between Ce and Si (Ce-O-Si) formed on $CeSi_2$ and $Mo_\alpha CeSi_2$ (Fig. S5), matching well with our previous report [21].

3.4. Redox properties and surface acidity

Topsøe et al. have reported that the NH_3-SCR reaction was composed of a redox cycle and an acid cycle [57]. Here, H_2-TPR experiments were conducted to evaluate the redox properties of $Mo_\alpha CeSi_2$ (Fig. 6). For CeO_2, the peak α at *ca.* 544 °C and the peak β at *ca.* 780 °C could be assigned to the reduction of surface oxygen species/Ce^{4+} and bulk Ce^{4+} respectively [14]. While for $CeSi_2$ and $Mo_\alpha CeSi_2$, the intensity of peak α significantly enhanced, indicating the drastically improved reduction degree. The missing peak β on $CeSi_2$ and $Mo_\alpha CeSi_2$ suggested the formation of ultra-small CeO_2 particles, well supported by the results of XRD and Raman spectra. Furthermore, for $Mo_\alpha CeSi_2$ with the optimal Mo doping amount ($Mo_{0.1}CeSi_2$), peak α shifted to the lower temperatures from 545 °C to 521 °C, which meant that the redox capability of $CeSi_2$ was further improved by Mo doping.

NH_3-TPD profiles for $CeSi_2$ and $Mo_{0.1}CeSi_2$ were collected to further estimate the impact of Mo doping on the surface acidity. The fitted parameters could be found in Table S3. As shown in Fig. 7a, after Mo doping, a higher desorption amount was observed on $Mo_{0.1}CeSi_2$ (0.82 mmol/$g_{cat.}$) when compared with that on $CeSi_2$ (0.45 mmol/$g_{cat.}$), related to the formation of more acid sites on $Mo_{0.1}CeSi_2$. Peak α and β could be attributed to the NH_3 adsorbed on Ce or Si sites. Much more intensive desorption peak at *ca.* 250 °C on $Mo_{0.1}CeSi_2$ (Peak γ) was mainly assigned to NH_3 species bounded to Mo sites, suggesting that Mo doping could further promote the strength of acid sites. More acid sites with higher strength could be one of the reasons for the improved NH_3-SCR activity on $Mo_{0.1}CeSi_2$. *In situ* DRIFTS of NH_3 adsorption was also conducted on $Mo_{0.1}CeSi_2$ to investigate the types of acid sites (Figs. 7b and S6). The bands at *ca.* 1460 cm^{-1} and *ca.* 1646 cm^{-1} could be assigned to the NH_4^+ species bound to Brønsted acid sites [14,21,58,59], while the relatively weaker band at *ca.* 1563 cm^{-1} was attributed to NH_3 on Lewis acid sites [46], well supported by our previous report that Brønsted acid sites were much more than Lewis acid sites on MoO_3-CeO_2 catalyst with highly dispersed Mo species [60]. No distinct difference in the type of acid sites was observed on $Mo_{0.1}CeSi_2$ and $CeSi_2$. As reported

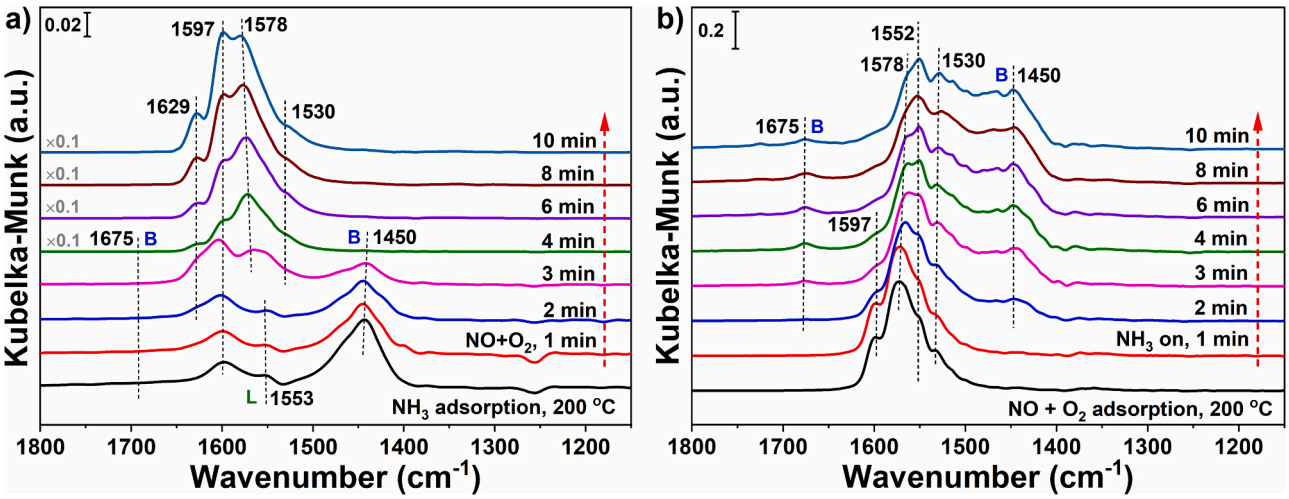

Fig. 9. a) *In situ* DRIFTS of NO + O_2 reacting with pre-adsorbed NH_3 on $Mo_{0.1}CeSi_2$ at 200 °C; b) *In situ* DRIFTS of NH_3 reacting with pre-adsorbed NO + O_2 on $Mo_{0.1}CeSi_2$ at 200 °C.

elsewhere, highly dispersed Mo species could serve as Brønsted acid sites [42,44,53], which well supported the results of NH_3-TPD and *in situ* DRIFTS of NH_3 adsorption.

3.5. NO/NH_3-oxidation

To further reveal the effect of Mo doping on $CeSi_2$, NO/NH_3 oxidation activity test on $Mo_{0.1}CeSi_2$ and $CeSi_2$ was conducted. As illustrated in Fig. 8a, higher NO oxidation efficiency was observed on $Mo_{0.1}CeSi_2$ than on $CeSi_2$. It has been widely reported that the NH_3-SCR activity could get enhanced by the *in situ* oxidation of NO to NO_2 by following a "fast SCR" mechanism [61,62]. The higher NO oxidation activity on $Mo_{0.1}CeSi_2$ suggested that Mo doping could promote the low-temperature NH_3-SCR activity on $CeSi_2$ by facilitating the NO oxidation to NO_2. Also, a higher NH_3 oxidation activity was achieved on $Mo_{0.1}CeSi_2$, suggesting the more efficient activation of NH_3 (Fig. 8b). Interestingly, although the NH_3 oxidation activity on $Mo_{0.1}CeSi_2$ was higher than that on $CeSi_2$, the N_2 selectivity was still maintained at a high level (>90%). As discussed in the previous section, the better redox properties on $Mo_{0.1}CeSi_2$ might contribute to its higher NO_x/NH oxidation activity, then dramatically improved low-temperature NH_3-SCR activity.

3.6. Reaction mechanism

The reaction mechanism on $Mo_{0.1}CeSi_2$ was investigated by *in situ* DRIFTS experiments. Firstly, to identify the reactivity of adsorbed NH_3, NO + O_2 was introduced into the samples pre-adsorbed with NH_3 (Fig. 9a). It was observed that the bands assigned to the adsorbed NH_4^+ (1450 cm^{-1} and 1675 cm^{-1}) decreased rapidly with the introduction of NO + O_2 in the first 4 min, and several bands ascribed to gaseous NO_2 (1629 cm^{-1}), bridging bidentate nitrates (1597 cm^{-1}), chelating bidentate nitrate (1578 cm^{-1}), and monodentate nitrates (1530 cm^{-1}) emerged [63–65], indicating that adsorbed NH_3 species was the efficient active species in the NH_3-SCR reaction. More acid sites on $Mo_{0.1}CeSi_2$ could make a great contribution to its enhanced NH_3-SCR activity. To further investigate the reactivity of adsorbed NO_x, *in situ* DRIFTS of NH_3 reacting with pre-adsorbed NO + O_2 was conducted (Fig. 9b). After being exposed to NH_3, although the band at 1597 cm^{-1} assigned to bridging bidentate nitrates vanished rapidly, the bands at *ca.* 1530 cm^{-1} enhanced significantly, indicating the deformation of bidentate nitrates to monodentate nitrates instead of consumption by NH_3 [14]. For the bands at 1578 and 1552 cm^{-1} (chelating bidentate nitrates), no obvious change was observed even after 10 min of exposure to NH_3. In short summary, adsorbed nitrates on $Mo_{0.1}CeSi_2$ were inert in the NH_3-SCR reaction. The NH_3-SCR reaction on $Mo_{0.1}CeSi_2$ followed an efficient Eley-Rideal (E-R) mechanism, in which the adsorbed NH_3 species could react with gaseous NO_x efficiently [37,66].

4. Conclusions

In this work, based on a CeO_2-SiO_2 catalyst with superior SO_2 resistance ability, we developed a novel Mo doped CeO_2-SiO_2 catalyst with improved low-temperature activity. After being doped with the appropriate amount of Mo, the redox properties and surface acidity of $CeSi_2$ were greatly enhanced, which could facilitate the activation of reactants and the adsorption of active NH_3 species on $Mo_{0.1}CeSi_2$. By following an efficient E-R mechanism, better NH_3-SCR performance was achieved on $Mo_{0.1}CeSi_2$. $Mo_{0.1}CeSi_2$ also exhibited superior resistance to SO_2/H_2O poisoning. This work provided a simple and effective strategy to prepare an efficient Mo-Ce-Si mixed-oxide catalyst with great resistance to SO_2 poisoning.

CRediT authorship contribution statement

Wei Tan: Methodology, Investigation, Formal analysis, Visualization, Writing – original draft. **Jin Wang**: Investigation. **Yandi Cai**: Investigation. **Lulu Li**: Investigation. **Shaohua Xie**: Investigation. **Fei Gao**: Conceptualization, Writing – review & editing, Funding acquisition, Supervision. **Fudong Liu**: Conceptualization, Writing – review & editing, Funding acquisition, Supervision. **Lin Dong**: Investigation, Resources.

Declaration of Competing Interest

The authors declare that they have no known competing financial interests or personal relationships that could have appeared to influence the work reported in this paper.

Acknowledgements

The financial supports from the National Natural Science Foundation of China (No. 21972063) and Natural Science Foundation of Jiangsu Province (BK20200012) are gratefully acknowledged. F. Liu acknowledges the Startup Fund from the University of Central Florida (UCF). S. Xie acknowledges the Preeminent Postdoctoral Program (P3) at UCF.

Appendix A. Supporting information

Supplementary data associated with this article can be found in the online version at doi:10.1016/j.cattod.2021.07.007.

References

[1] I. Manisalidis, E. Stavropoulou, A. Stavropoulos, E. Bezirtzoglou, Environmental and health impacts of air pollution: A review, Front. Public Health 8 (2020) 14, https://doi.org/10.3389/fpubh.2020.00014.
[2] L. Wang, J. Wang, X. Tan, C. Fang, Analysis of NO_x pollution characteristics in the atmospheric environment in changchun city, Atmosphere 11 (2020) 30, https://doi.org/10.3390/atmos11010030.
[3] C. Jia, J. Gao, K.W. Huang, V. Jose, P. Thepsithar, J.-M. Lee, Selective catalytic reduction of NO_x in marine engine exhaust gas over supported transition metal oxide catalysts, Chem. Eng. J. 414 (2021), 128794, https://doi.org/10.1016/j.cej.2021.128794.
[4] Y. Liu, J. Zhao, J.-M. Lee, Conventional and new materials for selective catalytic reduction (SCR) of NO_x, ChemCatChem 10 (2018) 1499–1511, https://doi.org/10.1002/cctc.201701414.
[5] G. Busca, L. Lietti, G. Ramis, F. Berti, Chemical and mechanistic aspects of the selective catalytic reduction of NO_x by ammonia over oxide catalysts: a review, Appl. Catal. B 18 (1998) 1–36, https://doi.org/10.1016/S0926-3373(98)00040-X.
[6] J. Li, H. Chang, L. Ma, J. Hao, R.T. Yang, Low-temperature selective catalytic reduction of NO_x with NH_3 over metal oxide and zeolite catalysts—A review, Catal. Today 175 (2011) 147–156, https://doi.org/10.1016/j.cattod.2011.03.034.
[7] H. Wang, J. Li, K. Li, Y. Lin, J. Chen, L. Gao, V. Nicolosi, X. Xiao, J.-M. Lee, Transition metal nitrides for electrochemical energy applications, Chem. Soc. Rev. 50 (2021) 1354–1390, https://doi.org/10.1039/D0CS00415D.
[8] K. Elouarzaki, V. Kannan, V. Jose, H.S. Sabharwal, J.-M. Lee, Recent trends, benchmarking, and challenges of electrochemical reduction of CO_2 by molecular catalysts, Adv. Energy Mater. 9 (2019), 1900090, https://doi.org/10.1002/aenm.201900090.
[9] P. Prabhu, V. Jose, J.-M. Lee, Design strategies for development of TMD-based heterostructures in electrochemical energy systems, Matter 2 (2020) 526–553, https://doi.org/10.1016/j.matt.2020.01.001.
[10] B. Wang, M. Wang, L. Han, Y. Hou, W. Bao, C. Zhang, G. Feng, L. Chang, Z. Huang, J. Wang, Improved activity and SO_2 resistance by Sm-modulated redox of $MnCeSmTiO_x$ mesoporous amorphous oxides for low-temperature NH_3-SCR of NO, ACS Catal. 10 (2020) 9034–9045, https://doi.org/10.1021/acscatal.0c02567.
[11] S. Xie, Z. Wang, W. Tan, Y. Zhu, S. Collier, L. Ma, S.N. Ehrlich, P. Xu, Y. Yan, T. Xu, J. Deng, F. Liu, Highly active and stable palladium catalysts on novel ceria-alumina supports for efficient oxidation of carbon monoxide and hydrocarbons, Environ. Sci. Technol. 55 (2021) 7624–7633, https://doi.org/10.1021/acs.est.1c00077.
[12] L. Han, S. Cai, M. Gao, J.-y Hasegawa, P. Wang, J. Zhang, L. Shi, D. Zhang, Selective catalytic reduction of NO_x with NH_3 by using novel catalysts: state of the art and future prospects, Chem. Rev. 119 (2019) 10916–10976, https://doi.org/10.1021/acs.chemrev.9b00202.
[13] W. Qu, X. Liu, J. Chen, Y. Dong, X. Tang, Y. Chen, Single-atom catalysts reveal the dinuclear characteristic of active sites in NO selective reduction with NH_3, Nat. Commun. 11 (2020) 1–7, https://doi.org/10.1038/s41467-020-15261-5.
[14] W. Tan, J. Wang, L. Li, A. Liu, G. Song, K. Guo, Y. Luo, F. Liu, F. Gao, L. Dong, Gas phase sulfation of ceria-zirconia solid solutions for generating highly efficient and SO_2 resistant NH_3-SCR catalysts for NO removal, J. Hazard. Mater. 388 (2020), 121729, https://doi.org/10.1016/j.jhazmat.2019.121729.
[15] W. Shan, F. Liu, Y. Yu, H. He, The use of ceria for the selective catalytic reduction of NO_x with NH_3, Chin. J. Catal. 35 (2014) 1251–1259, https://doi.org/10.1016/S1872-2067(14)60155-8.
[16] C. Tang, H. Zhang, L. Dong, Ceria-based catalysts for low-temperature selective catalytic reduction of NO with NH_3, Catal. Sci. Technol. 6 (2016) 1248–1264, https://doi.org/10.1039/C5CY01487E.
[17] Paolo Fornasiero, Tiziano Montini, Michele Melchionna, Matteo Monai, Fundamentals and catalytic applications of CeO_2-based materials, Chem. Rev. 116 (2016) 5987–6041, https://doi.org/10.1021/acs.chemrev.5b00603.
[18] A. Trovarelli, Catalytic properties of ceria and CeO_2-containing materials, Catal. Rev. Sci. Eng. 38 (1996) 439–520, https://doi.org/10.1080/01614949608006464.
[19] X. Hu, J. Chen, W. Qu, R. Liu, D. Xu, Z. Ma, X. Tang, Sulfur-resistant ceria-based low-temperature SCR catalysts with the non-bulk electronic states of ceria, Environ. Sci. Technol. 55 (2021) 5435–5441, https://doi.org/10.1021/acs.est.0c08736.
[20] L. Ma, C.Y. Seo, M. Nahata, X. Chen, J. Li, J.W. Schwank, Shape dependence and sulfate promotion of CeO_2 for selective catalytic reduction of NO_x with NH_3, Appl. Catal. B 232 (2018) 246–259, https://doi.org/10.1016/j.apcatb.2018.03.065.
[21] W. Tan, A. Liu, S. Xie, Y. Yan, T.E. Shaw, Y. Pu, K. Guo, L. Li, S. Yu, F. Gao, F. Liu, L. Dong, Ce-Si mixed oxide: a high sulfur resistant catalyst in the NH_3-SCR reaction through the mechanism-enhanced process, Environ. Sci. Technol. 55 (2021) 4017–4026, https://doi.org/10.1021/acs.est.0c08410.
[22] L. Zhang, J. Sun, Y. Xiong, X. Zeng, C. Tang, L. Dong, Catalytic performance of highly dispersed WO_3 loaded on CeO_2 in the selective catalytic reduction of NO by NH_3, Chin. J. Catal. 38 (2017) 1749–1758, https://doi.org/10.1016/S1872-2067(17)62887-0.
[23] Z. Ma, D. Weng, X. Wu, Z. Si, Effects of WO_x modification on the activity, adsorption and redox properties of CeO_2 catalyst for NO_x reduction with ammonia, J. Environ. Sci. 24 (2012) 1305–1316, https://doi.org/10.1016/S1001-0742(11)60925-X.
[24] Z. Ma, X. Wu, Z. Si, D. Weng, J. Ma, T. Xu, Impacts of niobia loading on active sites and surface acidity in NbO_x/CeO_2-ZrO_2 NH_3-SCR catalysts, Appl. Catal. B 179 (2015) 380–394, https://doi.org/10.1016/j.apcatb.2015.05.038.
[25] D. Wang, Y. Peng, Q. Yang, F. Hu, J. Li, J. Crittenden, NH_3-SCR performance of WO_3 blanketed CeO_2 with different morphology: balance of surface reducibility and acidity, Catal. Today 332 (2019) 42–48, https://doi.org/10.1016/j.cattod.2018.07.048.
[26] Q. Wu, X. Chen, J. Mi, S. Cai, L. Ma, W. Zhao, J. Chen, J. Li, The absence of oxygen in sulfation promotes the performance of the sulfated CeO_2 catalyst for low-temperature selective catalytic reduction of NO_x by NH_3: redox property versus acidity, ACS Sustain. Chem. Eng. 9 (2021) 967–979, https://doi.org/10.1021/acssuschemeng.0c08427.
[27] L. Chen, J. Li, M. Ge, DRIFT study on cerium-tungsten/titiania catalyst for selective catalytic reduction of NO_x with NH_3, Environ. Sci. Technol. 44 (2010) 9590–9596, https://doi.org/10.1021/es102692b.
[28] L. Chen, J. Li, M. Ge, R. Zhu, Enhanced activity of tungsten modified CeO_2/TiO_2 for selective catalytic reduction of NO_x with ammonia, Catal. Today 153 (2010) 77–83, https://doi.org/10.1016/j.cattod.2010.01.062.
[29] X. Zhao, L. Huang, H. Li, H. Hu, X. Hu, L. Shi, D. Zhang, Promotional effects of zirconium doped $CeVO_4$ for the low-temperature selective catalytic reduction of NO_x with NH_3, Appl. Catal. B 183 (2016) 269–281, https://doi.org/10.1016/j.apcatb.2015.10.052.
[30] S. Yang, Y. Guo, H. Chang, L. Ma, Y. Peng, Z. Qu, N. Yan, C. Wang, J. Li, Novel effect of SO_2 on the SCR reaction over CeO_2: Mechanism and significance, Appl. Catal. B 136 (2013) 19–28, https://doi.org/10.1016/j.apcatb.2013.01.028.
[31] T. Gu, Y. Liu, X. Weng, H. Wang, Z. Wu, The enhanced performance of ceria with surface sulfation for selective catalytic reduction of NO by NH_3, Catal. Commun. 12 (2010) 310–313, https://doi.org/10.1016/j.catcom.2010.10.003.
[32] L. Zhang, W. Zou, K. Ma, Y. Cao, Y. Xiong, S. Wu, C. Tang, F. Gao, L. Dong, Sulfated temperature effects on the catalytic activity of CeO_2 in NH_3-selective catalytic reduction conditions, J. Phys. Chem. C 119 (2015) 1155–1163, https://doi.org/10.1021/jp511282c.
[33] H. Xu, J. Liu, Z. Zhang, S. Liu, Q. Lin, Y. Wang, S. Dai, Y. Chen, Design and synthesis of highly-dispersed WO_3 catalyst with highly effective NH_3-SCR activity for NO_x abatement, ACS Catal. 9 (2019) 11557–11562, https://doi.org/10.1021/acscatal.9b03503.
[34] Y. Peng, K. Li, J. Li, Identification of the active sites on CeO_2-WO_3 catalysts for SCR of NO_x with NH_3: an *in situ* IR and Raman spectroscopy study, Appl. Catal. B 140 (2013) 483–492, https://doi.org/10.1016/j.apcatb.2013.04.043.
[35] W. Shan, F. Liu, H. He, X. Shi, C. Zhang, Novel cerium-tungsten mixed oxide catalyst for the selective catalytic reduction of NO_x with NH_3, Chem. Commun. 47 (2011) 8046–8048, https://doi.org/10.1039/C1CC12168E.
[36] S. Ding, F. Liu, X. Shi, H. He, Promotional effect of Nb additive on the activity and hydrothermal stability for the selective catalytic reduction of NO_x with NH_3 over $CeZrO_x$ catalyst, Appl. Catal. B 180 (2016) 766–774, https://doi.org/10.1016/j.apcatb.2015.06.055.
[37] Z. Ma, X. Wu, H. Härelind, D. Weng, B. Wang, Z. Si, NH_3-SCR reaction mechanisms of $NbO_x/Ce_{0.75}Zr_{0.25}O_2$ catalyst: DRIFTS and kinetics studies, J. Mol. Catal. A: Chem. 423 (2016) 172–180, https://doi.org/10.1016/j.molcata.2016.06.023.
[38] L. Yan, Y. Liu, K. Zha, H. Li, L. Shi, D. Zhang, Deep insight into the structure-activity relationship of Nb modified SnO_2-CeO_2 catalysts for low-temperature selective catalytic reduction of NO by NH_3, Catal. Sci. Technol. 7 (2017) 502–514, https://doi.org/10.1039/C6CY02242A.
[39] Z. Liu, H. Su, J. Li, Y. Li, Novel MoO_3/CeO_2-ZrO_2 catalyst for the selective catalytic reduction of NO_x by NH_3, Catal. Commun. 65 (2015) 51–54, https://doi.org/10.1016/j.catcom.2015.02.028.
[40] X. Tang, Y. Shi, F. Gao, S. Zhao, H. Yi, Z. Xie, Promotional role of Mo on $Ce_{0.3}FeO_x$ catalyst towards enhanced NH_3-SCR catalytic performance and SO_2 resistance, Chem. Eng. J. 398 (2020), 125619, https://doi.org/10.1016/j.cej.2020.125619.
[41] M. Iwasaki, K. Dohmae, Y. Nagai, E. Sudo, T. Tanaka, Experimental assessment of the bifunctional NH_3-SCR pathway and the structural and acid-base properties of WO_3 dispersed on CeO_2 catalysts, J. Catal. 359 (2018) 55–67, https://doi.org/10.1016/j.jcat.2017.12.032.
[42] S. Ding, F. Liu, X. Shi, K. Liu, Z. Lian, L. Xie, H. He, Significant promotion effect of Mo additive on a novel Ce-Zr mixed oxide catalyst for the selective catalytic reduction of NO_x with NH_3, ACS Appl. Mater. Interfaces 7 (2015) 9497–9506, https://doi.org/10.1021/acsami.5b00636.
[43] L. Li, C. Ge, J. Ji, W. Tan, X. Wang, X. Wei, K. Guo, C. Tang, L. Dong, Effects of different methods of introducing Mo on denitration performance and anti-SO_2 poisoning performance of CeO_2, Chin. J. Catal. 42 (2021) 1488–1499, https://doi.org/10.1016/S1872-2067(20)63778-0.
[44] L. Li, P. Li, W. Tan, K. Ma, W. Zou, C. Tang, L. Dong, Enhanced low-temperature NH_3-SCR performance of $CeTiO_x$ catalyst via surface Mo modification, Chin. J. Catal. 41 (2020) 364–373, https://doi.org/10.1016/S1872-2067(19)63437-6.
[45] X. Li, X. Li, J. Li, J. Hao, Identification of the arsenic resistance on MoO_3 doped CeO_2/TiO_2 catalyst for selective catalytic reduction of NO_x with ammonia, J. Hazard. Mater. 318 (2016) 615–622, https://doi.org/10.1016/j.jhazmat.2016.07.058.
[46] Z. Liu, S. Zhang, J. Li, L. Ma, Promoting effect of MoO_3 on the NO_x reduction by NH_3 over CeO_2/TiO_2 catalyst studied with *in situ* DRIFTS, Appl. Catal. B 144 (2014) 90–95, https://doi.org/10.1016/j.apcatb.2013.06.036.
[47] W. Tan, J. Wang, S. Yu, A. Liu, L. Li, K. Guo, Y. Luo, S. Xie, F. Gao, F. Liu, L. Dong, Morphology-sensitive sulfation effect on ceria catalysts for NH_3-SCR, Top. Catal. 63 (2020) 932–943, https://doi.org/10.1007/s11244-020-01342-8.

[48] A. Nikolenko, V. Strelchuk, O. Gnatyuk, P. Kraszkiewicz, V. Boiko, E. Kovalska, W. Mista, R. Klimkiewicz, V. Karbivskii, G. Dovbeshko, *In situ* Raman study of laser-induced stabilization of reduced nanoceria (CeO_{2-x}) supported on graphene, J. Raman Spectrosc. 50 (2019) 490–498, https://doi.org/10.1002/jrs.5542.

[49] S. Loridant, Raman spectroscopy as a powerful tool to characterize ceria-based catalysts, Catal. Today (2020), https://doi.org/10.1016/j.cattod.2020.03.044 (in press).

[50] Y. Wu, G. Hu, Y. Xie, M. Guo, M. Luo, Solid state reaction of MoO_3-CeO_2 complex oxide studied by Raman spectroscopy, Solid State Sci. 13 (2011) 2096–2099, https://doi.org/10.1016/j.solidstatesciences.2011.08.005.

[51] E.L. Lee, I.E. Wachs, *In situ* Raman spectroscopy of SiO_2-supported transition metal oxide catalysts: an isotopic ^{18}O–^{16}O exchange study, J. Phys. Chem. C 112 (2008) 6487–6498, https://doi.org/10.1021/jp076485w.

[52] A. Retsinas, A.G. Kalampounias, G.N. Papatheodorou, Glass formation and Raman spectra of CaO-SiO_2 glasses towards the orthosilicate limit, J. Phys. Chem. Solids 99 (2016) 19–24, https://doi.org/10.1016/j.jpcs.2016.08.001.

[53] L. Li, W. Tan, X. Wei, Z. Fan, A. Liu, K. Guo, K. Ma, S. Yu, C. Ge, C. Tang, L. Dong, Mo doping as an effective strategy to boost low temperature NH_3-SCR performance of CeO_2/TiO_2 catalysts, Catal. Commun. 114 (2018) 10–14, https://doi.org/10.1016/j.catcom.2018.05.015.

[54] L. Qi, Q. Yu, Y. Dai, C. Tang, L. Liu, H. Zhang, F. Gao, L. Dong, Y. Chen, Influence of cerium precursors on the structure and reducibility of mesoporous CuO-CeO_2 catalysts for CO oxidation, Appl. Catal. B 119–120 (2012) 308–320, https://doi.org/10.1016/j.apcatb.2012.02.029.

[55] T. Dai, X. Fan, Y. Ren, S. Hou, Y. Zhang, L. Qian, Y. Li, X. Liu, Layer-controlled synthesis of wafer-scale $MoSe_2$ nanosheets for photodetector arrays, J. Mater. Sci. 53 (2018) 8436–8444, https://doi.org/10.1007/s10853-018-2142-6.

[56] N. Yan, F. Wang, H. Zhong, Y. Li, Y. Wang, L. Hu, Q. Chen, Hollow porous SiO_2 nanocubes towards high-performance anodes for lithium-ion batteries, Sci. Rep. 3 (2013) 1568, https://doi.org/10.1038/srep01568.

[57] N.-Y. Topsøe, Mechanism of the selective catalytic reduction of nitric oxide by ammonia elucidated by *in situ* on-line fourier transform infrared spectroscopy, Science 265 (1994) 1217–1219, https://doi.org/10.1126/science.265.5176.1217.

[58] Y. Yu, W. Tan, D. An, C. Tang, W. Zou, C. Ge, Q. Tong, F. Gao, J. Sun, L. Dong, NKCC1 promotes EMT-like process in GBM via RhoA and Rac1 signaling pathways, J. Cell. Physiol. 234 (2019) 1630–1642, https://doi.org/10.1016/j.cattod.2019.12.025 (in press).

[59] X. Yao, L. Chen, J. Cao, F. Yang, W. Tan, L. Dong, Morphology and crystal-plane effects of CeO_2 on TiO_2/CeO_2 catalysts during NH_3-SCR reaction, Ind. Eng. Chem. Res. 57 (2018) 12407–12419, https://doi.org/10.1021/acs.iecr.8b02830.

[60] J. Zhu, F. Gao, L. Dong, W. Yu, L. Qi, Z. Wang, L. Dong, Y. Chen, Studies on surface structure of M_xO_y/MoO_3/CeO_2 system (M=Ni, Cu, Fe) and its influence on SCR of NO by NH_3, Appl. Catal. B 95 (2010) 144–152, https://doi.org/10.1016/j.apcatb.2009.12.021.

[61] W. Shan, F. Liu, H. He, X. Shi, C. Zhang, A superior Ce-W-Ti mixed oxide catalyst for the selective catalytic reduction of NO_x with NH_3, Appl. Catal. B 115–116 (2012) 100–106, https://doi.org/10.1016/j.apcatb.2011.12.019.

[62] P. Forzatti, I. Nova, E. Tronconi, Enhanced NH_3 selective catalytic reduction for NO_x abatement, Angew. Chem. Int. Ed. 48 (2009) 8366–8368, https://doi.org/10.1002/anie.200903857.

[63] W.S. Kijlstra, D.S. Brands, E.K. Poels, A. Bliek, Mechanism of the selective catalytic reduction of NO by NH_3 over MnO_x/Al_2O_3, I. Adsorption and desorption of the single reaction components, J. Catal. 171 (1997) 208–218, https://doi.org/10.1006/jcat.1997.1788.

[64] X. Yao, R. Zhao, L. Chen, J. Du, C. Tao, F. Yang, L. Dong, Selective catalytic reduction of NO_x by NH_3 over CeO_2 supported on TiO_2: Comparison of anatase, brookite, and rutile, Appl. Catal. B 208 (2017) 82–93, https://doi.org/10.1016/j.apcatb.2017.02.060.

[65] J.L. Flores-Moreno, G. Delahay, F. Figueras, B. Coq, DRIFTS study of the nature and reactivity of the surface compounds formed by co-adsorption of NO, O_2 and propene on sulfated titania-supported rhodium catalysts, J. Catal. 236 (2005) 292–303, https://doi.org/10.1016/j.jcat.2005.10.002.

[66] Y. Yu, W. Tan, D. An, X. Wang, A. Liu, W. Zou, C. Tang, C. Ge, Q. Tong, J. Sun, L. Dong, Insight into the SO_2 resistance mechanism on γ-Fe_2O_3 catalyst in NH_3-SCR reaction: a collaborated experimental and DFT study, Appl. Catal. B: Environ. 281 (2021), 119544, https://doi.org/10.1016/j.apcatb.2020.119544.